Autofluorescence Imaging With Near-Infrared Excitation: Normalization by Reflectance to Reduce Signal From Choroidal Fluorophores

Artur V. Cideciyan, Malgorzata Swider, and Samuel G. Jacobson

Scheie Eye Institute, Department of Ophthalmology, Perelman School of Medicine at the University of Pennsylvania, Philadelphia, Pennsylvania, United States

Correspondence: Artur V. Cideciyan, Scheie Eye Institute, University of Pennsylvania, 51 N. 39th Street, Philadelphia, PA 19104, USA; cideciya@mail.med.upenn.edu.

Submitted: February 22, 2015
Accepted: April 10, 2015

Citation: Cideciyan AV, Swider M, Jacobson SG. Autofluorescence imaging with near-infrared excitation: normalization by reflectance to reduce signal from choroidal fluorophores. *Invest Ophthalmol Vis Sci*. 2015;56:3393–3406. DOI:10.1167/iovs.15-16726

Purpose. We previously developed reduced-illuminance autofluorescence imaging (RAFI) methods involving near-infrared (NIR) excitation to image melanin-based fluorophores and short-wavelength (SW) excitation to image lipofuscin-based flurophores. Here, we propose to normalize NIR-RAFI in order to increase the relative contribution of retinal pigment epithelium (RPE) fluorophores.

Methods. Retinal imaging was performed with a standard protocol holding system parameters invariant in healthy subjects and in patients. Normalized NIR-RAFI was derived by dividing NIR-RAFI signal by NIR reflectance point-by-point after image registration.

Results. Regions of RPE atrophy in Stargardt disease, AMD, retinitis pigmentosa, choroideremia, and Leber congenital amaurosis as defined by low signal on SW-RAFI could correspond to a wide range of signal on NIR-RAFI depending on the contribution from the choroidal component. Retinal pigment epithelium atrophy tended to always correspond to high signal on NIR reflectance. Normalizing NIR-RAFI reduced the choroidal component of the signal in regions of atrophy. Quantitative evaluation of RPE atrophy area showed no significant differences between SW-RAFI and normalized NIR-RAFI.

Conclusions. Imaging of RPE atrophy using lipofuscin-based AF imaging has become the gold standard. However, this technique involves bright SW lights that are uncomfortable and may accelerate the rate of disease progression in vulnerable retinas. The NIR-RAFI method developed here is a melanin-based alternative that is not absorbed by opsins and bisretinoid moieties, and is comfortable to view. Further development of this method may result in a nonmydriatic and comfortable imaging method to quantify RPE atrophy extent and its expansion rate.

Keywords: autofluorescence, melanin, lipofuscin, infrared

The retina is a complex layered structure of neurons and glia that lines the inside surface of the eyeball. Photoreceptor cells form the most distal layer of the retina and their outer segments interdigitate with the apical portion of a monolayer of retinal pigment epithelium (RPE) cells that provide support. The basal surface of the RPE is separated from the choroidal blood supply by Bruch's membrane. Imaging of the retina, RPE, and the choroid is an important component of the diagnosis of ocular disorders affecting these tissues. The retina is nearly transparent, but both the RPE and choroid contain pigments that strongly interact with imaging lights across a range of wavelengths. The two major pigments of the RPE are lipofuscin and melanin.[1–3] The choroid also contains melanin with optical and biochemical properties as well as an embryonic origin that differs from its RPE counterpart.[4–8]

One of the imaging modalities used in diagnosing the health of the RPE and its response to treatments is fundus autofluorescence (FAF) imaging.[9–11] In its traditional form, FAF imaging is performed with a bright short-wavelength light, which provides information mostly originating from lipofuscin pigments in the RPE.[12–14] Especially with regards to delineation of the area of geographic atrophy in AMD and its change over time, FAF has become an accepted outcome measure in clinical trials (e.g., NCT00890097, NCT01527500 in the public domain, www.clinicaltrials.gov). There are however several drawbacks to FAF imaging. First, vulnerable retinas in animal models of retinal degenerative conditions demonstrate increased sensitivity to light levels[15–20] that are otherwise thought to be harmless to normal retinas. FAF involves one of the brighter lights used in clinical examination of patients. The evidence of hypersensitivity to light damage in patients with retinal disease, at least in certain retinal 'sectors,' has been circumstantial,[16,21,22] but if it were true, FAF imaging could potentially confound studies of natural history or intervention in vulnerable patients. Especially important are younger patients who are increasingly taking part in clinical trials and may be more vulnerable due to greater transmission of shorter wavelength lights through young lenses.[23,24] In addition to vulnerable patients, exposure limits for normal retinas have come under question recently.[25–27] Second, subjects feel uncomfortable with the bright light and tend to squint and tear, which tends to reduce image quality. This factor makes it very difficult to record images in patients with photoaversion especially in primary cone diseases such as cone dystrophy, achromatopsia, or blue-cone monochroma-

tism. Third, the normal FAF signal near the fovea is very low making it difficult to detect RPE disturbance limited to the foveal region.[28] Fourth, non-RPE fluorophores could complicate the interpretation of the images.[29–31] Fifth, imaging with FAF tends to depress subsequent visual function measures, especially in patients with slow dark-adaptation kinetics.[32–40] Sixth, FAF imaging requires pupillary dilation; nonmydriatic imaging is not possible.

An alternative form of AF imaging based on near-infrared (NIR) excitation light[41] has been proposed by three independent groups, and variably named "fundus near infrared fluorescence,"[42] "near-infrared autofluorescence," or "AF [787],"[43] or "reduced-illuminance autofluorescence imaging with NIR excitation (NIR-RAFI)."[44] The latter method was one of two RAFI methods we proposed, the other being short-wavelength (SW)-RAFI.[44] NIR-RAFI and similar NIR-based methods have the distinct advantage of being low-illuminance (i.e., the patients perceive it as a dim red light unlike the bright SW light used in traditional FAF imaging). More importantly, the excitation wavelength is far from the absorption maxima of opsin and bisretinoid moieties that are thought to be involved in some forms of light damage,[45–47] and thus it could be considered "safer" for susceptible retinas at least in terms of actinic wavelengths.

NIR-RAFI is thought to be originating from melanin and related pigments located within the RPE and the choroid.[48] One of the drawbacks of NIR-RAFI include the lack of widespread availability of imaging equipment capable of recording this signal. Nevertheless, a growing literature now exists from our group[28,44,48–58] and that of others[31,41–43,59–72] on the use of NIR-RAFI, and the interpretation of the acquired images in different retinal conditions. Importantly, SW excited AF imaging modalities and NIR-RAFI provide overlapping but independent information about RPE and retinal abnormalities.[31,44,59,61,65,68] Sometimes, interpretation of NIR-RAFI is complicated due to existence of relevant melanin-based fluorophores both within the RPE and choroid layers. This complexity is especially obvious in cases when the RPE is atrophied, and the resulting 'window' allows detection of the choroidal signal. A method to preferentially enhance the relative contribution of the RPE melanin could simplify interpretation of the resulting images. Current work describes the reflectance-normalized RAFI (RAFIn) that provides greater contrast between RPE and choroidal sources of fluorescence, at least under certain conditions. Further optimization of this technique could allow nonmydriatic imaging and quantification of RPE atrophy as well as greater understanding less severe RPE 'disease,' which often involves changes in pigmentation.

Methods

Subjects

All procedures followed the Declaration of Helsinki and the study was approved by the institutional review board. Informed consent, assent and parental permission were obtained and the work was HIPAA compliant. Included were patients ($n = 27$) with Stargardt disease (STGD1), AMD, retinitis pigmentosa (RP), choroideremia (CHM), or Leber congenital amaurosis (LCA; Supplementary Table S1), and healthy subjects ($n = 18$).

Retinal Imaging

Imaging was performed with a confocal scanning laser ophthalmoscope (Spectralis HRA; Heidelberg Engineering, Heidelberg, Germany) to obtain three types of en face images. SW-RAFI used 486-nm excitation and collection of emission signals over approximately 500 to 750 nm. The laser power was set at 25% using a software modification provided by the manufacturer as compared with a recalibration we had performed in earlier work.[44] The detector sensitivity setting was either 87% or 105%. Near-infrared–reflectance (NIR-REF) imaging was performed with 815-nm light with a 25% laser power setting and a detector sensitivity of 55%. In CHM patients, detector sensitivity was further reduced as low as to 40% in order to avoid saturation. NIR-RAFI was performed with 786-nm light and emission signals were collected between approximately 810 and 900 nm. Laser output setting was 100% and detector sensitivity was 87% or 105%.

All images were acquired with the high speed mode wherein a 30° × 30° square field was sampled onto 768 × 768 pixels. The dilated pupil of the subject was aligned with the optical axis of the instrument (head position stabilized with chin and forehead rests) in a room with dimmed ambient lights. Focus setting was optimized first under NIR reflectance. Minor adjustments to focus were made under AF images in order to obtain the highest intensity. Manufacturer's ART feature was used whenever possible with a 21 frame average; manufacturer's automatic normalization feature was turned off. When necessary, a wide-field image montage was assembled by manually specifying retinal landmark pairs corresponding to each other in overlapping segments using custom-written software (MATLAB 6.5, Natick, MA, USA). Images from left eyes were transformed into equivalent right eyes for comparability. Eyes with blue, gray, green, and hazel irides were classified as "light colored" and those with brown irides were classified as "dark colored."

NIR-RAFI and SW-RAFI images were black-level corrected by subtracting the frame-specific black-level recorded by the acquisition software. NIR-RAFIn was calculated by first registering the NIR-REF and NIR-RAFI images using a custom program (MATLAB 6.5) with user-selection of corresponding landmarks distributed throughout the image and allowing for linear spatial transformation between the images being registered. Next, NIR-RAFI image was divided by NIR-REF, pixel by pixel to produce NIR-RAFIn. In order to quantify and plot NIR-RAFIn signals, profiles along the horizontal and vertical meridians were calculated along a 10-pixel wide band. In a subset of patients, cross-sectional optical coherence tomography (OCT) imaging was also available. In a group of STGD1 patients, the apparent contrast between RPE atrophy and neighboring nonatrophy region was calculated as the mean gray level difference divided by the mean gray level sum, after subtracting relevant black-level values. Contrast was calculated for NIR-RAFIn and SW-RAFI, and compared. Also, the areas of RPE atrophy were quantified on NIR-RAFIn and SW-RAFI, and compared.

Results

Detecting RPE Atrophy With Autofluorescence Imaging

Retinal pigment epithelial cells naturally contain at least two types of fluorophores: those related to melanin that fluoresce upon excitation with NIR light and those related to lipofuscin that fluoresce upon excitation with SW light. In the macula of healthy subjects, NIR-RAFI and SW-RAFI signals are dominated by RPE melanin and lipofuscin distribution, respectively (Figs. 1A, 1B). Specifically, normal SW-RAFI shows a low signal near the fovea mostly due to the absorption of the SW light by macular pigment surrounded by a higher signal that reaches an elliptical annular peak near approximately 10° to 17° eccentricity (see Ref. 55 for quantification of SW-RAFI signal across a wide retinal extent) corresponding closely to the highest density of rod photoreceptors.[73] NIR-RAFI, on the other hand,

Investigative Ophthalmology & Visual Science

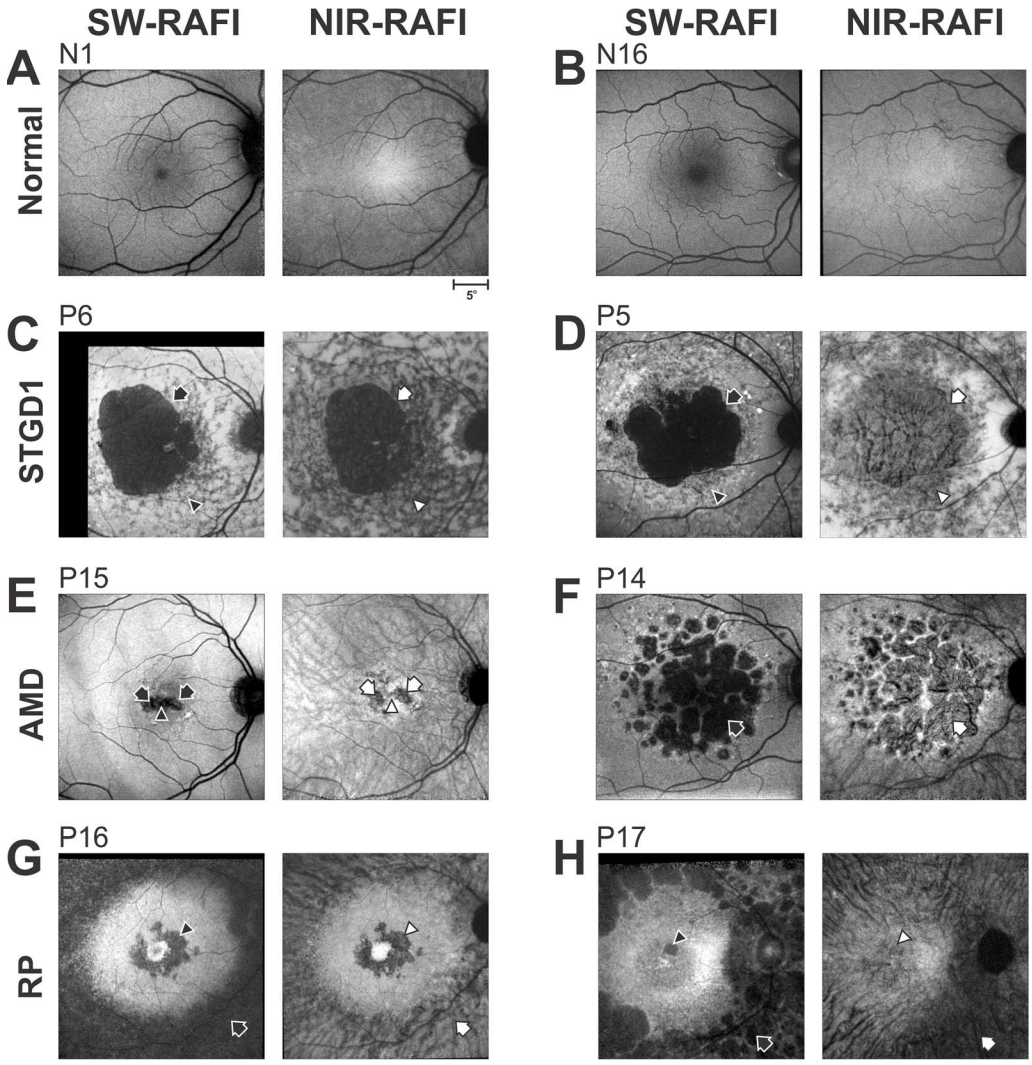

Figure 1. Reduced-illuminance autofluorescence imaging (RAFI) results comparing SW- and NIR-excitation in healthy eyes and in retinal disease. (**A**, **B**) Reduced-illuminance autofluorescence in a representative young normal (N1) with dark irides and in an older normal (N16) with light irides. Calibration (*lower right*) applies to all images. (**C**, **D**) Stargardt disease with large central RPE atrophy in patients with light (P6) or dark (P5) irides. *Arrows*, superonasal boundary between atrophy and neighboring healthier region. *Arrowheads*, heterogenous-appearing region infero-nasal to fovea. (**E**, **F**) Nonneovascular AMD with geographic atrophy in two patients (P15, P14) with dark irides. *Arrows*, regions of geographic atrophy. *Arrowhead*, foveal preservation in P15. (**G**, **H**) Retinitis pigmentosa with parafoveal and perimacular degeneration in two patients (P16, P17) with light irides. *Arrows*, inferonasal perimacular region with RPE disease. *Arrowheads*, parafoveal region with RPE atrophy. Image contrasts are individually adjusted for visibility of features.

shows a high signal near the fovea likely due to the higher melanin optical density resulting from taller cell bodies and greater melanin concentration within these RPE cells.

In retinal disease, upon atrophy of RPE cells, fluorescence originating from RPE melanin and lipofuscin is extinguished. The remnant signals recorded at retinal loci with RPE atrophy could be due to unmasking of choroidal or scleral signal. Alternatively or additionally, minor retinal fluorophores[30,74,75] or pseudofluorescence could contribute. Examples of RPE atrophy demonstrate the range of results obtained in different patient phenotypic categories with SW or NIR illumination (Figs. 1C–H). A 34-year-old patient P6 with STGD1 shows a large region of RPE atrophy with low signal on SW-RAFI (Fig. 1C, black arrow); surrounding the atrophy is a heterogeneous region of high and low signal (Fig. 1C, black arrowhead). On NIR-RAFI, the region of atrophy also demonstrates a low signal (Fig. 1C, white arrow); surrounding the atrophy is a heterogeneous region of low and intermediate signal (Fig. 1C, white arrowhead). A 32-year-old STGD1 patient P5 also shows a large region of RPE atrophy on SW-RAFI (Fig. 1D, black arrow) surrounded by a heterogeneous region of high and low signal (black arrowhead). Surprisingly, on NIR-RAFI there is very little loss of signal at the region corresponding to the atrophy; instead, there is a region where the blood vessel pattern appears choroidal in origin (Fig. 1D, white arrow). P6 had light whereas P5 had dark colored irides, and thus the greater appearance of choroidal features in P5 appears consistent with correlation previously observed between choroidal pigmentation and eye color.[3,31,43] An 80-year-old AMD patient P15 with geographic atrophy shows what appears to be a horizontally-elongated region with loss of SW-RAFI signal (Fig. 1E, black arrows). On NIR-RAFI, on the other hand, there are two parafoveal circular regions of signal loss (Fig. 1E, white arrows), and relative preservation of the fovea between the two regions (Fig. 1E, white arrowhead). A 75-year-old AMD patient P14 with geographic atrophy shows loss of AF signal on

Investigative Ophthalmology & Visual Science

SW-RAFI (Fig. 1F, black arrow) but not NIR-RAFI (white arrow); at the retinal loci with RPE atrophy on SW-RAFI, a choroidal pattern of blood vessels is visible on NIR-RAFI. Both patients had dark irides.

Patients with RP tend to lose (mid-) peripheral retina to progressive retinal degeneration first. In some RP patients, there can also be macular changes relatively early in the disease.[76] A 25-year-old patient P16 with X-linked RP (XLRP) shows a macular region of high signal surrounded by an annulus of atrophy on SW-RAFI (Fig. 1G, black arrow); there is also a distinct bull's eye u-shaped darkness at the parafoveal region (Fig. 1G, black arrowhead). On NIR-RAFI, macular appearance has distinct similarities to that of SW-RAFI demonstrating the retained signal in foveal and perifoveal regions, with the loss of signal at the parafovea (Fig. 1G, white arrowhead). The paramacular region on NIR-RAFI shows a distinctly choroidal appearance (Fig. 1G, white arrow) and differs from the dark SW-RAFI result. P16 had light colored irides, which is consistent with the lack of choroidal signal parafoveally but it is not consistent with a strong choroidal signal in the paramacular region. A different RP patient, P17, also shows relative retention of the macular region with parafoveal involvement (Fig. 1H, black arrowhead). However, the NIR-RAFI result is distinctly different with substantial choroidal structure apparent throughout the central retina. Appearance of high choroidal signal is not consistent with the light-colored irides of P17.

These examples of differing macular and retinal degenerative diseases demonstrate that estimates of RPE health based on interpretation of SW-RAFI sometimes overlaps with that of NIR-RAFI. In complex cases with differing SW- and NIR-RAFI results, additional information is necessary to decipher sources and differentiate between melanin-based fluorophores of the RPE and choroid. Iris pigmentation is thought to be related to the choroidal pigmentation[3,31,43] and appears to explain some of the results but not others.

NIR Absorption and Backscatter in Retina, RPE, Choroid, and Sclera

Local contrast of anatomical features visible in reflectance imaging results from the interaction of the illumination light with local changes in scattering and absorption at those wavelengths, as well as the mode of imaging.[77–80] Melanin pigments in the RPE and choroid are the major contributors to both scattering as well as absorption of NIR light.[79] In some healthy eyes, NIR-reflectance imaging shows a relatively diffuse background interrupted by darker retinal blood vessels (Fig. 2A, left two panels). The relative lack of visible choroidal features in N4 with dark irides and N6 with light irides suggests that either NIR light is absorbed at the level of the RPE and does not traverse to deeper layers, or there is no backscatter originating from the choroid, or both. However, some healthy subjects do show choroidal features such as N7 (Fig. 2A, right panel, white arrow). Counterintuitively, N7 has light colored irides and presumably less choroidal melanin despite prominent choroidal features. Importantly, retinal regions showing choroidal features are often substantially brighter on NIR reflectance than neighboring regions showing no choroidal features. One hypothesis consistent with normal results is that RPE melanin has a predominant absorption property, whereas choroidal melanin has a predominant (back-) scattering property, at least for the wavelength (815 nm) and confocal imaging conditions used here. In line with this hypothesis, local visibility of the choroid with a brighter signal can result from one of two choices. First, local increases in choroidal melanin could cause relatively greater backscatter signal while overlying RPE has a uniform absorption. Second, local reductions in RPE melanin could cause relatively lower absorption, and thus unmask the backscatter signal originating from the choroid. There could also be a combination of both of these effects.

To evaluate these choices, we examined NIR reflectance in retinal degenerations. STGD1 patient P4 with a macular lesion showed a relatively dark ring of NIR-REF region corresponding to the parafovea, which was not atrophied based on SW-RAFI results (Fig. 2B, left panels, white arrowheads). There was however severe retinal degeneration at this location, and the relative loss of NIR backscatter signal can be due to the loss of photoreceptor outer segments and RPE apical processes. The lack of visibility of choroidal features despite OCT evidence of greater choroidal transmission of the NIR signal suggests that the absorption by the RPE melanin remains intact. STGD1 patients P7 and P12 with macular RPE atrophy (Fig. 2B), on the other hand, show a relative bright NIR-REF region corresponding to the loss of RPE, and likely loss of absorption component at the level of the RPE opening a window to detect the backscatter component from the choroid (or sclera). Optical coherence tomography scans show that transitions between dark to bright NIR-REF (white arrowheads) correspond to the increase of signal transmission into the choroid but choroidal thickness does not appear to change abruptly across the transition. Thus, the brighter NIR-REF signal is likely originating from the choroid as opposed to sclera.

Choroideremia is a disease of photoreceptors, RPE, and the choroid. The primary manifestation of the disease remains controversial but a direct, quantitative, and colocalized comparison has supported the hypothesis that the disease starts in photoreceptors.[81] NIR-REF signal in CHM eyes is often unusually high so that both laser power and detector sensitivity need to be substantially reduced in order to obtain unsaturated images. Different stages of CHM may contribute to the understanding of the sources contributing to the NIR-REF signal. P25 is a 38-year-old CHM patient (Fig. 2C, left) with evidence of retinal degeneration throughout the retina. NIR-REF, under standard recording conditions, results in a saturated image everywhere except for an irregular-shaped central region. NIR-REF signal within the center of the irregular region is normal but OCT shows substantial abnormalities at the level of the inner and outer segments, confirming previous results[81] that photoreceptor abnormalities precede melanin backscatter abnormalities. Partial degeneration of the photoreceptors within the immediate surrounds of the fovea corresponds to increased NIR-REF signal originating from the choroid (black arrow). Temporal to the optic nerve head in P25 and across most of the central retina in P27 (Fig. 2C) there is thinning of the choroid and likely greater contributions of NIR-REF signal coming from the sclera corresponding to retinal regions where choroidal blood vessels become invisible. P25 had dark irides and P27 light irides, thus showing a lack of a major correlation with eye color.

The examples of healthy, STGD1, and CHM eyes taken together could support the hypothesis that, with NIR light, choroidal melanin has a dominant backscatter component that can be unmasked by the reduction of the RPE melanin's absorption component that is in the normal light path of en face imaging.

Normalized NIR-RAFI: Results in Healthy Eyes

If choroidal melanin has a greater backscatter component than RPE melanin, it follows that the RPE component of the NIR-RAFI signal can be relatively enhanced by normalizing (dividing) by the NIR-REF signal. To test this hypothesis, NIR-REF and NIR-RAFI were obtained in 15 healthy eyes (ages 14–72 years) and normalized NIR-RAFI (NIR-RAFIn) was calculated. Figures 3A and 3B demonstrates the results in representative younger and older healthy subjects, respectively. NIR-REF

Investigative Ophthalmology & Visual Science

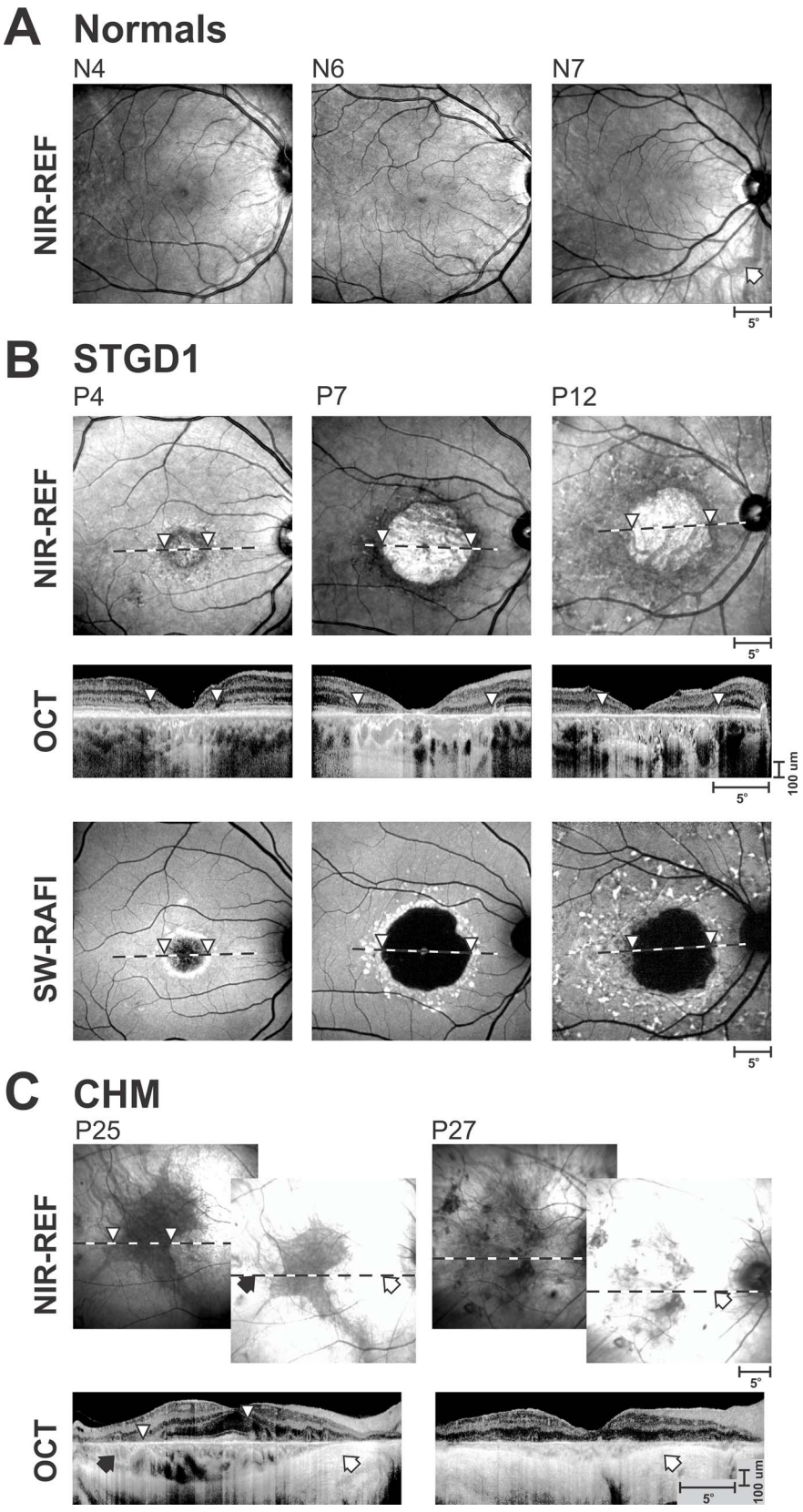

Figure 2. Range of reflectance (REF) images with NIR illumination showing different appearances of RPE and choroid likely associated with differences in absorption and backscatter at different depths. (**A**) Healthy subjects showing no obvious choroidal features (N4, dark irides), barely visible choroidal features (N6, light irides), and clearly visible choroidal features (N7, light irides, *arrow*). (**B**) Stargardt patients (STGD1) with central lesions showing a parafoveal ring of low NIR-REF signal (P4, *arrowheads*), and those high to low NIR-REF transition at the border of RPE atrophy (P7, P12, *arrowheads*). All three patients had light irides. Optical coherence tomography (OCT) and SW-RAFI images are also shown. *Horizontal dashed lines* depict the location and extent of the OCT. (**C**) A patient (P25, dark irides) with choroideremia (CHM) demonstrating the

Investigative Ophthalmology & Visual Science

relationship between the relatively retained central retinal pigmentation corresponding to relatively low NIR-REF signal. Another CHM patient (P27, light irides) demonstrating NIR-REF in the case of chorioretinal degeneration. The brighter NIR-REF images were recorded with the standard sensitivity setting, whereas the dimmer images recorded with a reduced sensitivity. *White arrows*, retinal regions with no obvious photoreceptors or choroid remaining. *Black arrows*, retinal regions with retained choroidal structure but without detectable photoreceptors. *Arrowheads*, correspondence between the boundaries of the low NIR-REF signal and the associated OCT scans.

image of the 19-year-old N3 shows relative brightness nasal to the fovea and greater visibility of choroidal vessels compared with the temporal region (Fig. 3A, left panel). NIR-RAFI image shows a higher fluorescence from the foveal region compared with the rest of the image. Surrounding the fovea, there is relatively greater fluorescence on the temporal retina compared with the nasal retina. NIR-RAFIn image makes the nasal-temporal asymmetry more distinct. NIR-REF image of the 62-year-old N17 appears more uniform (Fig. 3B, left panel). Near-infrared–RAFI image is also more uniform with only a minor increase in fluorescence near the fovea. NIR-RAFIn image shows a small region of brightness at the fovea but otherwise a relatively uniform signal.

NIR-REF, NIR-RAFI, and NIR-RAFIn values were quantified. Initially, we obtained intensity profiles across the fovea along the horizontal and vertical meridians and formed averages for younger (14–40 years; $n = 7$) and older (48–72 y; $n = 8$) subjects (Fig. 3C). For NIR-REF, there was little change at the fovea or along the vertical profile; there was, however, a tendency for NIR-REF signal to increase with age in the temporal retina and decrease with age in the nasal retina. For NIR-RAFI, there was age-related decrease of the signal everywhere but the decrease appeared greater at the fovea compared with the rest of retina. Subjects of all ages showed a substantial temporal-nasal asymmetry. NIR-RAFIn showed age-related decreases at the fovea and temporal retina, whereas changes were less substantial across the rest of the retina.

To better understand spatial distribution of NIR-RAFIn, data were collected from four regions and plotted against age; there was no obvious contribution of iris color to the calculated NIR-RAFIn signal (Fig. 3D). At the fovea, NIR-RAFIn signal decreased with a linear slope of –0.18 per decade ($r = 0.77$; $P < 0.01$) and at the temporal retina with a slope of –0.13 per decade ($r = 0.69$; $P < 0.01$). In the nasal, superior, and inferior retinal locations, slopes were not significantly different than zero ($P \geq 0.05$). Under the assumption that age-related preretinal changes (such as increased scattering and absorption by the lens) effect proportionally both NIR-REF and NIR-RAFI, the age-related changes seen in NIR-RAFIn would be expected to correspond to changes at the RPE and/or retina.

Normalized NIR-RAFI: Results in Retinal Degeneration

Near-infrared–based imaging was performed in patients representing different hereditary retinal degeneration phenotypes chosen to contain retinal regions with RPE atrophy, which is traditionally apparent as a low signal region on SW-RAFI (Fig. 4). A 69-year-old STGD1 patient, P13, showed high NIR-REF signal corresponding to the large macular region surrounded by lower signal (Fig. 4A, left panel). Centrally, NIR-RAFI signal was low with a strong choroidal blood vessel appearance despite the patient having light color irides. The paramacular region had higher NIR-RAFI signal on average but with major heterogeneity (Fig. 4A, second panel). NIR-RAFIn resulted in a region of dark signal clearly demarcated from the surrounding region of brighter signal (Fig. 4A, third panel). SW-RAFI showed a classic STGD1 appearance with dark region presumably corresponding to RPE atrophy surrounded by brighter region with heterogeneity (Fig. 4A, right panel).

A 29-year-old STGD1 patient, P3, also with light irides, showed a central region of high NIR-REF signal, surrounded by lower NIR-REF signal (Fig. 4B, left panel). NIR-RAFI showed low signal with choroidal appearance centrally surrounded by a heterogeneous appearance of intermediate and higher signal (Fig. 4B, second panel). Calculation of NIR-RAFIn resulted in reduction of the signal from the central region and greater heterogeneity in the surrounding region (Fig. 4B, third panel). SW-RAFI showed a classic STGD1 appearance with a central dark region presumably corresponding to RPE atrophy surrounded by heterogeneous region (Fig. 4B, right panel).

Quantitative analyses were performed in 13 STGD1 patients with clearly demarcated regions of RPE atrophy (Supplementary Fig. S1A) in order to compare the contrast between the region of atrophy and its surrounds. Edge contrast (Supplementary Fig. S1B) values for NIR-RAFIn (0.70 ± 0.11) tended to be lower than that for SW-RAFI (0.78 ± 0.05), and this small but significant ($P = 0.01$; paired *t*-test) difference appeared to result from the hyperautofluorescence surrounding atrophy on SW-RAFI but not on NIR-RAFIn (Fig. 1C, 4A, Supplementary Fig. S1A). We also compared the areas of atrophy delineated with NIR-RAFIn and SW-RAFI modalities over a range of atrophy sizes. The results were very similar (Supplementary Fig. S1C) with no significant differences ($P = 0.23$; paired *t*-test).

Next, we considered retinal degenerations that tend to preserve the macula. A 51-year-old RP patient, P18, showed a central region of lower NIR-REF signal surrounded perimacularly with higher signal and choroidal blood vessel structure (Fig. 4C, left). NIR-RAFI image showed a central elliptical region of homogeneous signal surrounded by a heterogeneous region of somewhat greater signal strength interrupted by dark choroidal blood vessels (Fig. 4C, second panel). NIR-RAFIn surprisingly showed two distinctly demarcated central ellipses of high signal (Fig. 4C, third panel, arrowheads and arrows). Surrounding the two ellipses was a region of intermediate signal and, further peripherally, lower signal. SW-RAFI image showed normal-appearing central macular region with a low signal surrounded by a penumbra of higher signal, further surrounded by low signal; in the perimacular region, there was evidence of multiple regions of RPE dropout (Fig. 4C, right).

A 53-year-old CHM patient, P26, illustrated the dramatic differences between the irregular central region of relatively-low NIR-REF signal (which is quantitatively abnormally high) and a surrounding region of relatively high signal (Fig. 4D, left). Optical coherence tomography imaging (not shown) demonstrated a region of retained photoreceptors with abnormal inner/outer segments corresponding to the region with the relatively-low NIR-REF signal, and no remaining photoreceptors in the regions with relatively high signal; there was abnormally high penetration of signal into the choroid. NIR-RAFI imaging showed relatively equal signal intensity across the macula, but there was much greater visibility of choroidal vessels in surrounding regions compared with the irregular central region (Fig. 4D, second panel, arrows). NIR-RAFIn resulted in a well differentiated central brighter region and darker surrounding region (Fig. 4D, third panel) and this was similar to the SW-RAFI results (Fig. 4D, right). Curiously, choroidal blood vessels appeared dark in NIR-RAFI but relatively bright on SW-RAFI modality.

Investigative Ophthalmology & Visual Science

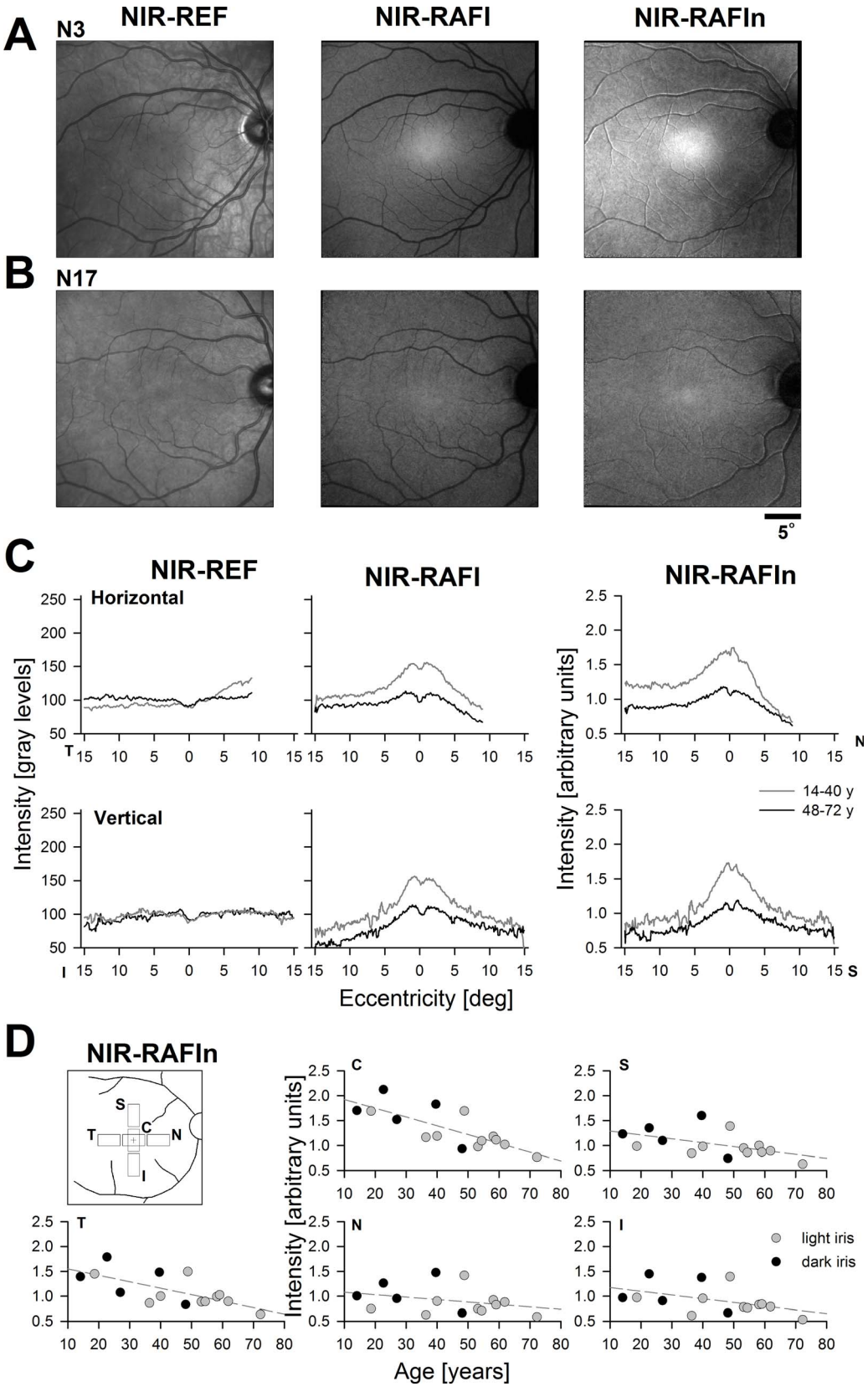

Figure 3. Quantitation of NIR-REF, NIR-RAFI, and NIR-RAFIn signals in a group of healthy subjects. (**A**, **B**) Representative results in younger (N3) and older (N17) healthy subjects. Both had lighter irides. (**C**) Mean horizontal and vertical profiles of signal intensity in younger (*gray*) and older (*black*) subjects. (**D**) NIR-RAFIn signal at five central locations (*Inset*, C, central; S, superior; I, inferior; T, temporal; N, nasal) across all healthy subjects as a function of age and eye color. *Dashed lines* depict linear regression.

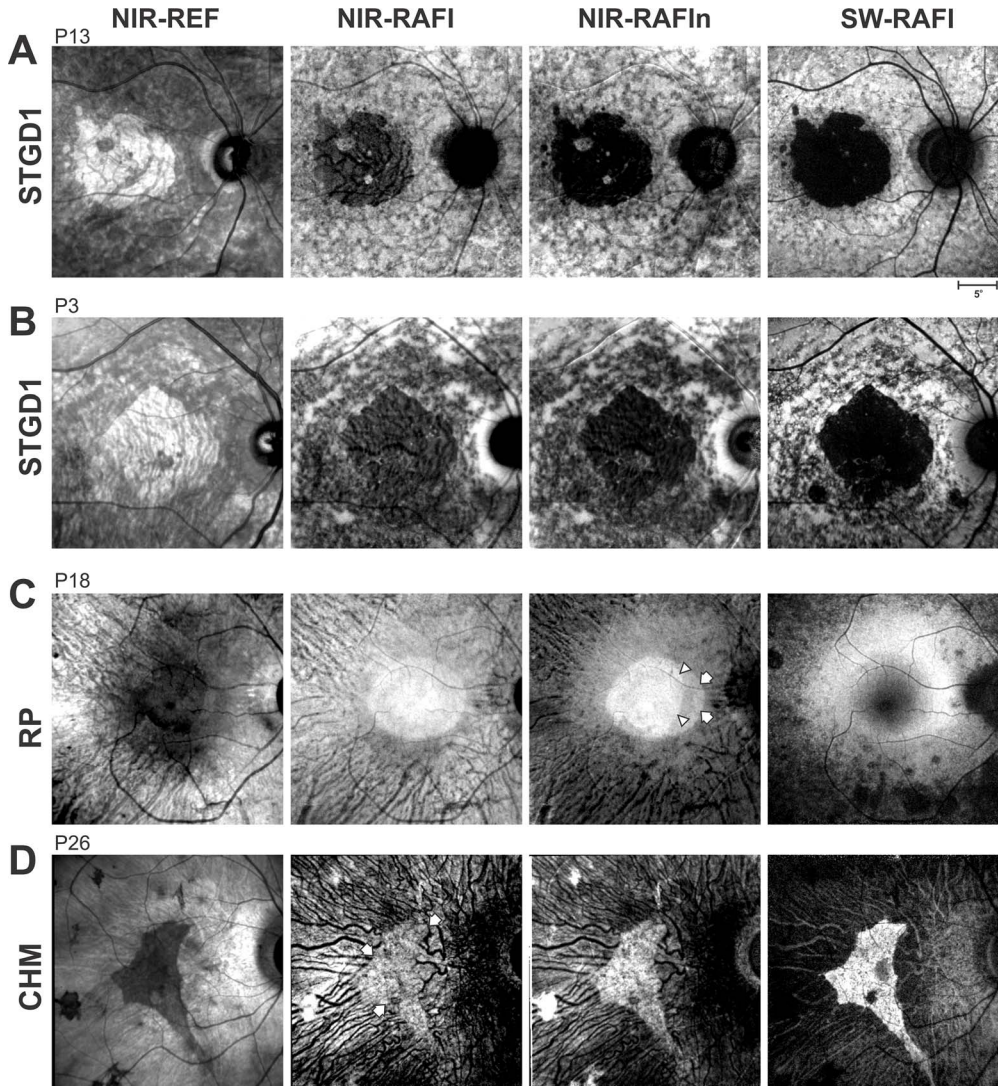

Figure 4. Comparison of RPE atrophy and neighboring healthier retina obtained with NIR modalities versus SW-RAFI in different retinal diseases. Representative examples of STGD1 patients with light irides (**A**, **B**), RP patient with dark irides (**C**), and CHM patient with light irides (**D**) are shown. NIR-REF image of the CHM patient is obtained with nonstandard detector sensitivity in order to avoid saturation. Calibration shown on lower right applies to all panels.

These results suggest that NIR-REF and NIR-RAFI provide key information about regional differences in melanization; in some conditions, melanization abnormalities are identical or similar to lipofuscin abnormalities, but in other conditions, there are important differences. NIR-RAFIn combines the NIR-REF and NIR-RAFI information in a manner that can be useful in estimating the RPE health.

Use of NIR Imaging in Eyes Where SW Lights Cannot Be Used

Leber congenital amaurosis caused by *RPE65* mutations has garnered a lot of attention due to the success of gene therapy treatment. Since gene therapy aims to restore the visual cycle in the RPE, it should be directed to regions with evidence of retained RPE (as well as overlying photoreceptors). The standard method of determining RPE atrophy using SW lights is complicated by the lack of the normal lipofuscin accumulation in this human disease[55,82] and its animal models.[83] An alternative method of determining the distribution of the RPE in *RPE65*-LCA eyes is to take advantage of the melanin fluorophores.

NIR-RAFIn results in two patients with *RPE65*-LCA are shown (Fig. 5A). An 18-year-old P23 with light irides shows a central region of high signal near the fovea likely corresponding to healthier RPE (Fig. 5A, upper). Temporal, superior, and superotemporal to the fovea has better retention of signal compared with inferonasal region; the latter likely corresponds to RPE atrophy or depigmentation. A 21-year-old P24 with dark irides shows a thin horizontally extended region of higher signal at the fovea surrounded by a circular region of lower signal likely corresponding to RPE atrophy (Fig. 5A, lower). In the temporal, superior, and inferior perifoveal regions, there is a return of NIR-RAFIn signal implying greater retention of RPE as compared with the nasal retina. Curiously, a choroidal blood vessel pattern is more apparent in the light colored P23 compared with the dark colored P24. These examples suggest that NIR-RAFIn can provide information about the distribution of melanized RPE and point to regions of potential therapy in

Investigative Ophthalmology & Visual Science

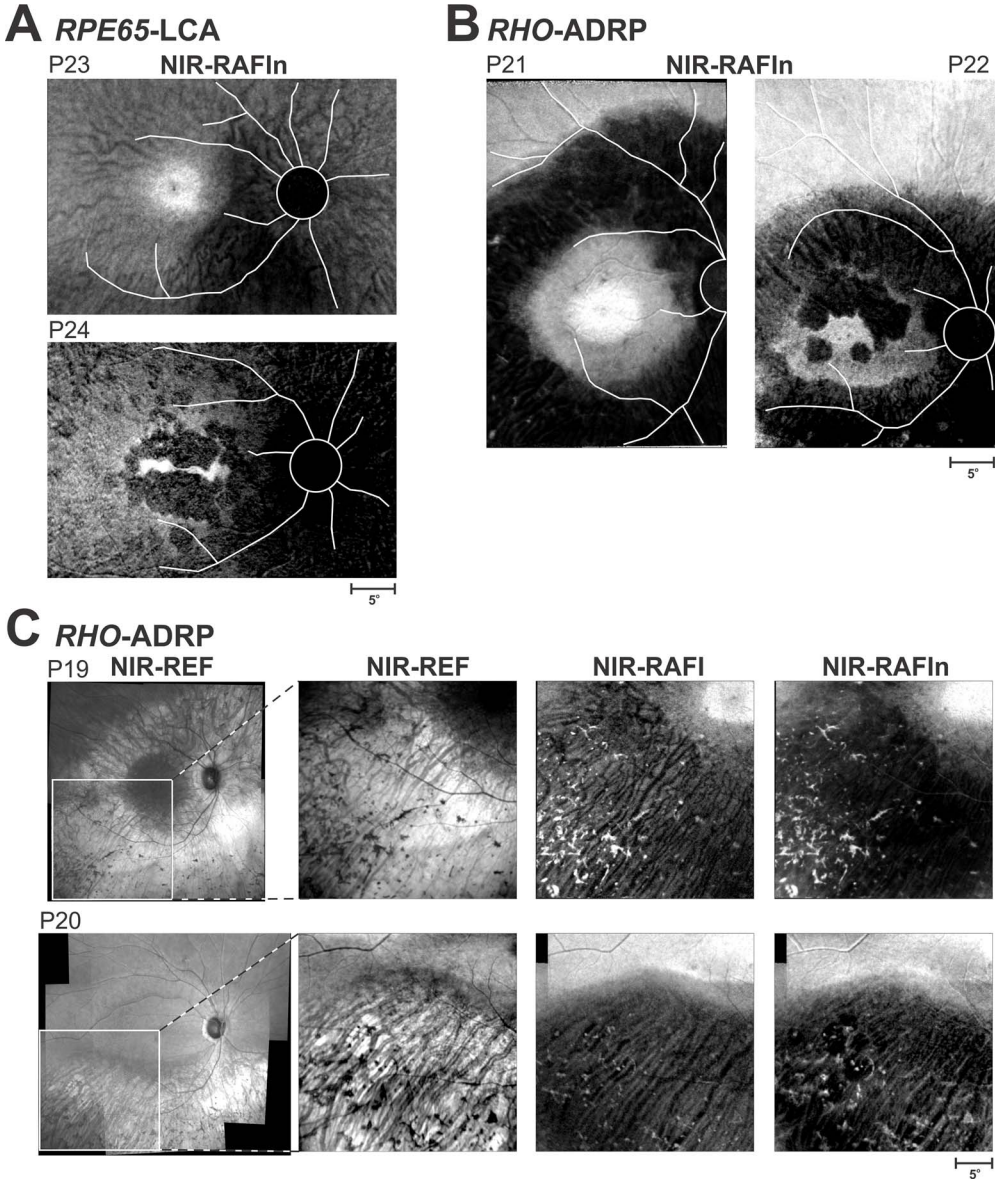

Figure 5. Imaging in *RPE65*-LCA and *RHO*-ADRP patients in whom SW-RAFI is not usable either because of the lack of lipofuscin resulting from underlying pathophysiology or because of concerns about the light load. (**A**) NIR-RAFIn results in *RPE65*-LCA patients P23 and P24. (**B**) NIR-RAFIn results in *RHO*-ADRP patients P21 and P22. Optic nerve head and major blood vessels are traced (*white*) to better interpret the context of the images shown. (**C**) Bone-spicule–like pigment in two patients with *RHO*-ADRP.

conditions where lipofuscin fluorophores cannot be used for this purpose.

Use of NIR Imaging in Eyes Where SW Lights Should Not Be Used

There has been accumulating evidence from a large number of animal models that some retinal degenerative conditions make retinas hypersensitive to lights such that illumination levels, that normally do not cause damage, can increase rates of retinal degeneration.[17] The most obviously vulnerable population is autosomal dominant RP (ADRP) patients with Class B *RHO* mutations.[22] Supportive evidence derives from dramatic hypersensitivity to light damage found in a naturally occurring *RHO*-mutant dog,[16] and in genetically engineered rodent[15,18–20] and frog[84] models. Figure 5B shows the NIR-RAFIn results in two patients with *RHO*-ADRP with Class B mutations. In each case, there appears to be very clear differentiation between retinal regions of higher NIR-RAFIn signal likely corresponding to retained RPE melanization and regions of lower NIR-RAFIn signal likely corresponding to RPE atrophy. These examples suggest that NIR-RAFIn can be used to define the natural history of progression of RPE disease in *RHO*-ADRP without undue risk from SW lights.

Evaluation of Bone-Spicule–Like Pigment With NIR-RAFI

An important pathognomic sign of RP is the funduscopic appearance in the midperiphery of bone-spicule–like pigment (BSP), which microscopically have been shown to be RPE cells that have detached from Bruch's membrane and migrated to the inner retina.[85] Bone-spicule–like pigment contains melanin but

not lipofuscin and tends to appear dark on NIR-REF; however, it is possible that BSP in different disease stages and/or caused by different genetic defects may have differences in terms of their optical backscatter and autofluorescence characteristics. Figure 5C shows NIR imaging in the inferior-temporal retina of two patients (both with light irides) with ADRP caused by a Class B *RHO* mutation. NIR-REF for both patients shows a region of high signal with visibility of choroidal blood vessels and overlying darker BSP (Fig. 5C, left two images). NIR-RAFI shows increased signal originating from the BSP overlying a darker signal with a choroidal pattern. Not unexpectedly, NIR-RAFIn enhances the contrast of the BSP in the region of RPE atrophy (Fig. 5C, right panel).

Discussion

Retinal degenerative conditions often involve a slow progression from a normal retina and RPE to partial loss of photoreceptors and abnormal pigmentation of the RPE, to dropout of RPE cells singly or in small clumps, to complete loss of photoreceptors as well as RPE.[86,87] In inherited retinal degenerations, this late stage of RPE disease is usually referred to as RPE atrophy, whereas in nonneovascular AMD, it is referred to as geographic atrophy. Historically, geographic atrophy was measured using color fundus photographs,[88,89] but the last decade has seen AF imaging using a SW excitation light become the new standard.[9,90–92] The definition of retinal regions representing RPE atrophy varies but in general it is thought to correspond to a well-defined zone of decreased autofluorescence with SW excitation. Current work also used this definition of RPE atrophy. Often such atrophy is surrounded by a penumbral region of signal heterogeneity, which likely includes RPE disease and even partial RPE loss. Previous studies have suggested that the extent of such abnormal heterogeneity visible with NIR AF exceeds the abnormality visible with SW AF.[31] Future studies extending the normalized NIR-RAFI method developed here from the macula to the extramacular regions together with colocalized OCT and visual function measures could shed further light into these transition zones.

Regions of RPE atrophy can appear over time, and already existing regions can expand. The total area covered by RPE atrophy has become an oft-used structural biomarker of macular disease because progression of macular atrophy area is associated with visual decline[93] and treatments slowing the growth of RPE atrophy would be expected to benefit patients' remaining vision. In order to obtain the best signal-to-noise ratio (especially in older eyes with age-related lens yellowing), a relatively high laser power is used is standard AF imaging. For most (younger) subjects, standard AF imaging lights are uncomfortably bright to view. Furthermore, there is a very large, and growing, literature in animal studies that suggests that bright lights may accelerate the rate of retinal degeneration in susceptible retinas.[15–20] We have previously proposed a SW-RAFI method with 4-fold reduction in laser power, which can still result in clinically and scientifically useful images,[44] especially in young and middle aged eyes with greater preretinal transmission and in older subjects with clear intraocular lenses. But even after 4-fold reduction, excitation lights remain uncomfortable to most subjects. An alternative AF imaging method based on NIR-excitation lights has been available for nearly a decade but difficulty in interpretation and delineation of regions of RPE atrophy has prevented widespread adoption of this technology. Here, we develop a version of this technology using both NIR reflectance and AF information that may provide a comfortable and safer imaging method to follow changes in RPE atrophy when evaluating the natural history of diseases or the effects of interventions. Upon further technical development, the form of imaging proposed here may even be performed without mydriatic agents.

Delineation of RPE Atrophy

On standard AF imaging with SW excitation light, RPE atrophy is thought to correspond to a region (or regions) of the retina with low signal separated with a sharply demarcated border from the surrounding regions of better preserved RPE with higher signal.[39,44,90–92,94] This definition of RPE atrophy is consistent with the hypothesis that SW-AF signal is dominated by lipofuscin fluorophores within the RPE. However, certain rare diseases such as *RPE65*-LCA demonstrate that it is possible for RPE to exist without lipofuscin. Other conditions such as *ABCA4*-STGD1 tend to substantially increase the SW-AF signal in otherwise healthy-appearing RPE making it difficult to judge what signal level corresponds to true RPE atrophy. And often enough, there are severe alterations of the RPE without frank atrophy. Thus, an alternative method for the delineation of RPE atrophy based on a different fluorophore could be useful. NIR-RAFI was previously proposed as an alternative[43,44] but existence of high choroidal melanin signals in some patients (Fig. 1) limited its usability for delineation of RPE atrophy. The novel normalization procedure highlighted in the current work may allow better contrast between regions of RPE atrophy and surrounding neighbors. However, larger studies will need to be performed to evaluate this hypothesis.

RPE Melanin Versus Choroidal Melanin

Melanin granules are prominent components of RPE cells and choroidal melanocytes.[1,4] Consistent with the different embryological origins (RPE cells from neuroectoderm and choroidal melanocytes from neural crest), there are differences in physical properties of these granules. RPE melanin granules are generally larger than choroidal granules[4] but both are of the same order of magnitude as the wavelength of the imaging lights used in this study. Within the RPE, there is further complexity in melanin distribution. Apical processes of the RPE contain elliptical granules aligned with their long axis parallel to the path of illumination, whereas the cytoplasm of the RPE contains elliptical granules mostly aligned with their long axis perpendicular to the path of illumination or spherical granules.[95] Apical/basal differences in scatter, absorption, and fluorescence possibly originating from differences in the interaction of light with intracellular melanin orientation is currently not known but could be attempted with realistic models of light propagation through the human retina, RPE, and choroid. Further to be considered are spatial, age-related, and cell-to-cell variations of pigmentation across RPE cells,[3,96–99] which could for example explain visibility of choroidal structures in some retinal regions but not others.

Eye Color and Choroidal Melanin

A classic study of healthy human autopsy eyes in 'black' and 'white' individuals showed similarity of RPE melanin but major differences in choroidal melanin[3]; lack of correlation between eye color and RPE melanin was independently confirmed.[96] Consistent with those findings were greater visibility of choroidal vessels in individuals with dark irides as compared with light irides when imaged with NIR-AF.[43] Our results show that choroidal blood vessel visibility can also be detected in some individuals with light irides (Figs. 2A, 4A, B). If our hypothesis of a greater NIR backscatter component originating from choroidal melanin, as compared with the RPE melanin, is confirmed independently, then our normalization method

Investigative Ophthalmology & Visual Science

proposed here may enrich the RPE melanin component of the NIR-RAFI signal independent of race and iris color.

Technical Issues and Further Development

NIR-REF and NIR-RAFI have been performed in the older HRA2 systems. Modern Spectralis HRA+OCT systems can also record NIR-REF and NIR-RAFI, however, the resulting NIR-RAFI signal is relatively low due to the limited passband remaining between approximately 790 and 840 nm to collect emission signals. Spectralis HRA systems (without OCT component), like the one used in the current work, are less commonly available but provide a wider emission passband extending to approximately 900 nm. The result is a greater signal to noise ratio. Ideally NIR-REF and NIR-RAFI should be acquired simultaneously such as with the interlaced scanning method used in all Spectralis systems. Then the high signal NIR-REF can be used to drive the real time registration and averaging functionality even in case of low NIR-RAFI signal. Currently, this is not possible because of the imbalance between 815-nm laser power (100 μW at the cornea) used for NIR-REF and the 786-nm laser power (3.8 mW at the cornea) used for NIR-RAFI; for a given detector sensitivity, either NIR-REF is saturated and NIR-RAFI is optimal, or NIR-REF is optimal and NIR-RAFI is too dim to be measurable. Substantial reduction of the laser power setting used for NIR-REF by the manufacturer would allow simultaneous acquisition.

In the current work, NIR-REF and NIR-RAFI were obtained sequentially with different detector sensitivities, and post processing was used to register and divide images pixel-by-pixel. The image registration process was not always perfect and resulted in ghosting of some of the blood vessels as a result. Simultaneous acquisition of NIR-REF and NIR-RAFI would not only provide better image registration, but also allow real-time display of the normalized result. Furthermore, use of NIR-REF signal for tracking would allow averaging of NIR-RAFI even under conditions of low signal. The latter may include nonmydriatic imaging, which would be expected to reduce both signals in proportion with the pupillary area, and, at least conceptually, the normalized result should be independent of pupil size and thus quantifiable.

Ideally, NIR-REF, NIR-RAFI, and OCT could be acquired simultaneously in order to make the most of cross-sectional data on retinal layers spatially locked to an image of melanin-based fluorophores of the RPE. For this purpose, 1060-nm OCT technology may have to be used so as to allow wider band of NIR-RAFI signal to be acquired.

Quantitative Measurements of Autofluorescence Signals

Most AF imaging results are interpreted qualitatively. Rare "quantitative" results have been obtained either by keeping the key system parameters (laser intensity and detector sensitivity) constant,[39,44,55,100,101] or by the use of an internal fluorescent reference.[31,102–104] Neither method however achieves true quantitation because of the unknown individual differences in terms of the loss of excitation and emission light through the preretinal transmission route; this effect can be especially prominent in aging eyes, which tend to absorb shorter wavelengths (yellow lenses) and scatter a broad range of wavelengths.[105–110] This shortcoming is relevant to imaging performed with either SW or NIR lights. The normalization procedure described here could, at least partially, compensate for differences in preretinal transmission losses along the light path and thus provide better quantitation. However, this feature remains to be evaluated when the technologic improvements allow simultaneous acquisition of both modalities.

Conclusions

Ideal technology provides an imaging system that distinguishes the regions of RPE health, alterations, disease, and frank atrophy in undilated eyes with comfortable lights during a short exam time without undue hazard potential. The normalized NIR-RAFI method developed here may be a first step toward the development of such a technology.

Acknowledgments

Supported by grants from the National Institutes of Health/National Eye Institutes (EY013203, EY017280, EY022012, EY017549; Bethesda, MD, USA), Pennsylvania Department of Health (Harrisburg, PA, USA), The Chatlos Foundation, Inc. (Longwood, FL, USA), and Foundation Fighting Blindness (Columbia, MD, USA).

Disclosure: **A.V. Cideciyan**, None; **M. Swider**, None; **S.G. Jacobson**, None

References

1. Feeney L. Lipofuscin and melanin of human retinal pigment epithelium. Fluorescence, enzyme cytochemical, and ultrastructural studies. *Invest Ophthalmol Vis Sci*. 1978;17:583–600.
2. Feeney-Burns L, Berman ER, Rothman H. Lipofuscin of human retinal pigment epithelium. *Am J Ophthalmol*. 1980;90:783–791.
3. Weiter JJ, Delori FC, Wing GL, Fitch KA. Retinal pigment epithelial lipofuscin and melanin and choroidal melanin in human eyes. *Invest Ophthalmol Vis Sci*. 1986;27:145–152.
4. Schraermeyer U, Heimann K. Current understanding on the role of retinal pigment epithelium and its pigmentation. *Pigment Cell Res*. 1999;12:219–236.
5. Boulton M, Dayhaw-Barker P. The role of the retinal pigment epithelium: topographical variation and ageing changes. *Eye (Lond)*. 2001;15(Pt 3):384–389.
6. Ward WC, Simon JD. The differing embryonic origins of retinal and uveal (iris/ciliary body and choroid) melanosomes are mirrored by their phospholipid composition. *Pigment Cell Res*. 2007;20:61–69.
7. Biesemeier A, Schraermeyer U, Eibl O. Chemical composition of melanosomes, lipofuscin and melanolipofuscin granules of human RPE tissues. *Exp Eye Res*. 2011;93:29–39.
8. Boulton ME. Studying melanin and lipofuscin in RPE cell culture models. *Exp Eye Res*. 2014;126:61–67.
9. Schmitz-Valckenberg S, Fleckenstein M, Scholl HP, Holz FG. Fundus autofluorescence and progression of age-related macular degeneration. *Surv Ophthalmol*. 2009;54:96–117.
10. Almeida A, Kaliki S, Shields CL. Autofluorescence of intraocular tumours. *Curr Opin Ophthalmol*. 2013;24:222–232.
11. Samy A, Lightman S, Ismetova F, Talat L, Tomkins-Netzer O. Role of autofluorescence in inflammatory/infective diseases of the retina and choroid. *J Ophthalmol*. 2014;2014:418193.
12. Delori FC. Spectrophotometer for noninvasive measurement of intrinsic fluorescence and reflectance of the ocular fundus. *Appl Opt*. 1994;33:7439–7452.
13. von Rückmann A, Fitzke FW, Bird AC. Distribution of fundus autofluorescence with a scanning laser ophthalmoscope. *Br J Ophthalmol*. 1995;79:407–412.
14. Delori FC, Dorey CK, Staurenghi G, Arend O, Goger DG, Weiter JJ. In vivo fluorescence of the ocular fundus exhibits retinal pigment epithelium lipofuscin characteristics. *Invest Ophthalmol Vis Sci*. 1995;36:718–729.
15. Wang M, Lam TT, Tso MO, Naash MI. Expression of a mutant opsin gene increases the susceptibility of the retina to light damage. *Vis Neurosci*. 1997;14:55–62.

16. Cideciyan AV, Jacobson SG, Aleman TS, et al. In vivo dynamics of retinal injury and repair in the rhodopsin mutant dog model of human retinitis pigmentosa. *Proc Natl Acad Sci U S A*. 2005;102:5233–5238.
17. Paskowitz DM, LaVail MM, Duncan JL. Light and inherited retinal degeneration. *Br J Ophthalmol*. 2006;90:1060–1066.
18. White DA, Fritz JJ, Hauswirth WW, Kaushal S, Lewin AS. Increased sensitivity to light-induced damage in a mouse model of autosomal dominant retinal disease. *Invest Ophthalmol Vis Sci*. 2007;48:1942–1951.
19. Valter K, Kirk DK, Stone J. Optimising the structure and function of the adult P23H-3 retina by light management in the juvenile and adult. *Exp Eye Res*. 2009;89:1003–1011.
20. Budzynski E, Gross AK, McAlear SD, et al. Mutations of the opsin gene (Y102H and I307N) lead to light-induced degeneration of photoreceptors and constitutive activation of phototransduction in mice. *J Biol Chem*. 2010;285:14521–14533.
21. Heckenlively JR, Rodriguez JA, Daiger SP. Autosomal dominant sectoral retinitis pigmentosa. Two families with transversion mutation in codon 23 of rhodopsin. *Arch Ophthalmol*. 1991;109:84–91.
22. Cideciyan AV, Hood DC, Huang Y, et al. Disease sequence from mutant rhodopsin allele to rod and cone photoreceptor degeneration in man. *Proc Natl Acad Sci U S A*. 1998;95:7103–7108.
23. Savage GL, Haegerstrom-Portnoy G, Adams AJ. Age changes in the optical density of human ocular media. *Clin Vis Sci*. 1993;8:97–108.
24. Guo Y, Tan J. Monte Carlo simulation of retinal light absorption by infants. *J Opt Soc Am A* 2015;32:271–276.
25. Morgan JI, Hunter JJ, Masella B, et al. Light-induced retinal changes observed with high-resolution autofluorescence imaging of the retinal pigment epithelium. *Invest Ophthalmol Vis Sci*. 2008;49:3715–3729.
26. Hunter JJ, Morgan JI, Merigan WH, Sliney DH, Sparrow JR, Williams DR. The susceptibility of the retina to photochemical damage from visible light. *Prog Retin Eye Res*. 2012;31:28–42.
27. Masella BD, Williams DR, Fischer WS, Rossi EA, Hunter JJ. Long-term reduction in infrared autofluorescence caused by infrared light below the maximum permissible exposure. *Invest Ophthalmol Vis Sci*. 2014;55:3929–3938.
28. Cideciyan AV, Hufnagel RB, Carroll J, et al. Human cone visual pigment deletions spare sufficient photoreceptors to warrant gene therapy. *Hum Gene Ther*. 2013;24:993–1006.
29. Birnbach CD, Järveläinen M, Possin DE, Milam AH. Histopathology and immunocytochemistry of the neurosensory retina in fundus flavimaculatus. *Ophthalmology*. 1994;101:1211–1219.
30. Elner VM, Park S, Cornblath W, Hackel R, Petty HR. Flavoprotein autofluorescence detection of early ocular dysfunction. *Arch Ophthalmol*. 2008;126:259–260.
31. Duncker T, Marsiglia M, Lee W, et al. Correlations among near-infrared and short-wavelength autofluorescence and spectral-domain optical coherence tomography in recessive Stargardt disease. *Invest Ophthalmol Vis Sci*. 2014;55:8134–8143.
32. Steinmetz RL, Haimovici R, Jubb C, Fitzke FW, Bird AC. Symptomatic abnormalities of dark adaptation in patients with age-related Bruch's membrane change. *Br J Ophthalmol*. 1993;77:549–554.
33. Cideciyan AV, Pugh EN Jr, Lamb TD, Huang Y, Jacobson SG. Rod plateaux during dark adaptation in Sorsby's fundus dystrophy and vitamin A deficiency. *Invest Ophthalmol Vis Sci*. 1997;38:1786–1794.
34. Cideciyan AV, Zhao X, Nielsen L, Khani SC, Jacobson SG, Palczewski K. Null mutation in the rhodopsin kinase gene slows recovery kinetics of rod and cone phototransduction in man. *Proc Natl Acad Sci U S A*. 1998;95:328–333.
35. Cideciyan AV, Haeseleer F, Fariss RN, et al. Rod and cone visual cycle consequences of a null mutation in the 11-cis-retinol dehydrogenase gene in man. *Vis Neurosci*. 2000;17:667–678.
36. Owsley C, Jackson GR, White M, Feist R, Edwards D. Delays in rod-mediated dark adaptation in early age-related maculopathy. *Ophthalmology*. 2001;108:1196–1202.
37. Jacobson SG, Cideciyan AV, Wright E, Wright AF. Phenotypic marker for early disease detection in dominant late-onset retinal degeneration. *Invest Ophthalmol Vis Sci*. 2001;42:1882–1890.
38. Haimovici R, Owens SL, Fitzke FW, Bird AC. Dark adaptation in age-related macular degeneration: relationship to the fellow eye. *Graefes Arch Clin Exp Ophthalmol*. 2002;240:90–95.
39. Cideciyan AV, Aleman TS, Swider M, et al. Mutations in ABCA4 result in accumulation of lipofuscin before slowing of the retinoid cycle: a reappraisal of the human disease sequence. *Hum Mol Genet*. 2004;13:525–534.
40. Jackson GR, Scott IU, Kim IK, Quillen DA, Iannaccone A, Edwards JG. Diagnostic sensitivity and specificity of dark adaptometry for detection of age-related macular degeneration. *Invest Ophthalmol Vis Sci*. 2014;55:1427–1431.
41. Piccolino FC, Borgia L, Zinicola E, Iester M, Torrielli S. Preinjection fluorescence in indocyanine green angiography. *Ophthalmology*. 1996;103:1837–1845.
42. Weinberger AW, Lappas A, Kirschkamp T, et al. Fundus near infrared fluorescence correlates with fundus near infrared reflectance. *Invest Ophthalmol Vis Sci*. 2006;47:3098–3108.
43. Keilhauer CN, Delori FC. Near-infrared autofluorescence imaging of the fundus: visualization of ocular melanin. *Invest Ophthalmol Vis Sci*. 2006;47:3556–3564.
44. Cideciyan AV, Swider M, Aleman TS, et al. Reduced-illuminance autofluorescence imaging in ABCA4-associated retinal degenerations. *J Opt Soc Am A Opt Image Sci Vis*. 2007;24:1457–1467.
45. Boulton M, Rózanowska M, Rózanowski B. Retinal photodamage. *J Photochem Photobiol B*. 2001;64:144–161.
46. Sparrow JR, Zhou J, Ben-Shabat S, Vollmer H, Itagaki Y, Nakanishi K. Involvement of oxidative mechanisms in blue-light-induced damage to A2E-laden RPE. *Invest Ophthalmol Vis Sci*. 2002;43:1222–1227.
47. Wenzel A, Grimm C, Samardzija M, Remé CE. Molecular mechanisms of light-induced photoreceptor apoptosis and neuroprotection for retinal degeneration. *Prog Retin Eye Res*. 2005;24:275–306.
48. Gibbs D, Cideciyan AV, Jacobson SG, Williams DS. Retinal pigment epithelium defects in humans and mice with mutations in MYO7A: imaging melanosome-specific autofluorescence. *Invest Ophthalmol Vis Sci*. 2009;50:4386–4393.
49. Cideciyan AV, Aleman TS, Jacobson SG, et al. Centrosomal-ciliary gene CEP290/NPHP6 mutations result in blindness with unexpected sparing of photoreceptors and visual brain: implications for therapy of Leber congenital amaurosis. *Hum Mutat*. 2007;28:1074–1083.
50. Aleman TS, Cideciyan AV, Sumaroka A, et al. Retinal laminar architecture in human retinitis pigmentosa caused by Rhodopsin gene mutations. *Invest Ophthalmol Vis Sci*. 2008;49:1580–1590.
51. Herrera W, Aleman TS, Cideciyan AV, et al. Retinal disease in Usher syndrome III caused by mutations in the clarin-1 gene. *Invest Ophthalmol Vis Sci*. 2008;49:2651–2660.
52. Aleman TS, Soumittra N, Cideciyan AV, et al. CERKL mutations cause an autosomal recessive cone-rod dystrophy with inner retinopathy. *Invest Ophthalmol Vis Sci*. 2009;50:5944–5954.

Investigative Ophthalmology & Visual Science

53. Jacobson SG, Aleman TS, Cideciyan AV, et al. Leber congenital amaurosis caused by Lebercilin (LCA5) mutation: retained photoreceptors adjacent to retinal disorganization. *Mol Vis*. 2009;15:1098–1106.
54. Jacobson SG, Cideciyan AV, Aleman TS, et al. Human retinal disease from AIPL1 gene mutations: foveal cone loss with minimal macular photoreceptors and rod function remaining. *Invest Ophthalmol Vis Sci*. 2011;52:70–79.
55. Cideciyan AV, Rachel RA, Aleman TS, et al. Cone photoreceptors are the main targets for gene therapy of NPHP5 (IQCB1) or NPHP6 (CEP290) blindness: generation of an all-cone Nphp6 hypomorph mouse that mimics the human retinal ciliopathy. *Hum Mol Genet*. 2011;20:1411–1423.
56. Dinculescu A, Estreicher J, Zenteno JC, et al. Gene therapy for retinitis pigmentosa caused by MFRP mutations: human phenotype and preliminary proof of concept. *Hum Gene Ther*. 2012;23:367–376.
57. Jacobson SG, Cideciyan AV, Huang WC, et al. TULP1 mutations causing early-onset retinal degeneration: preserved but insensitive macular cones. *Invest Ophthalmol Vis Sci*. 2014;55:5354–5364.
58. Jacobson SG, Cideciyan AV, Sumaroka A, Roman AJ, Wright AF. Late-onset retinal degeneration caused by C1QTNF5 mutation: sub-retinal pigment epithelium deposits and visual consequences. *JAMA Ophthalmol*. 2014;132:1252–1255.
59. Kellner U, Kellner S, Weinitz S. Chloroquine retinopathy: lipofuscin- and melanin-related fundus autofluorescence, optical coherence tomography and multifocal electroretinography. *Doc Ophthalmol*. 2008;116:119–127.
60. Theelen T, Boon CJ, Klevering BJ, Hoyng CB. Fundus autofluorescence in patients with inherited retinal diseases: patterns of fluorescence at two different wavelengths [in German]. *Ophthalmologe*. 2008;105:1013–1022.
61. Kellner S, Kellner U, Weber BH, Fiebig B, Weinitz S, Ruether K. Lipofuscin- and melanin-related fundus autofluorescence in patients with ABCA4-associated retinal dystrophies. *Am J Ophthalmol*. 2009;147:895–902, 902.e1.
62. Kellner U, Kellner S, Weber BH, Fiebig B, Weinitz S, Ruether K. Lipofuscin- and melanin-related fundus autofluorescence visualize different retinal pigment epithelial alterations in patients with retinitis pigmentosa. *Eye (Lond)*. 2009;23:1349–1359.
63. Kellner S, Weinitz S, Kellner U. Spectral domain optical coherence tomography detects early stages of chloroquine retinopathy similar to multifocal electroretinography, fundus autofluorescence and near-infrared autofluorescence. *Br J Ophthalmol*. 2009;93:1444–1447.
64. Ayata A, Tatlipinar S, Kar T, Unal M, Ersanli D, Bilge AH. Near-infrared and short-wavelength autofluorescence imaging in central serous chorioretinopathy. *Br J Ophthalmol*. 2009;93:79–82.
65. Kellner U, Kellner S, Weinitz S. Fundus autofluorescence (488 NM) and near-infrared autofluorescence (787 NM) visualize different retinal pigment epithelium alterations in patients with age-related macular degeneration. *Retina*. 2010;30:6–15.
66. Koizumi H, Maruyama K, Kinoshita S. Blue light and near-infrared fundus autofluorescence in acute Vogt-Koyanagi-Harada disease. *Br J Ophthalmol*. 2010;94:1499–1505.
67. Schmitz-Valckenberg S, Lara D, Nizari S, et al. Localisation and significance of in vivo near-infrared autofluorescent signal in retinal imaging. *Br J Ophthalmol*. 2011;95:1134–1139.
68. Cukras CA, Wong WT, Caruso R, Cunningham D, Zein W, Sieving PA. Centrifugal expansion of fundus autofluorescence patterns in Stargardt disease over time. *Arch Ophthalmol*. 2012;130:171–179.
69. Duncker T, Tabacaru MR, Lee W, Tsang SH, Sparrow JR, Greenstein VC. Comparison of near-infrared and short-wavelength autofluorescence in retinitis pigmentosa. *Invest Ophthalmol Vis Sci*. 2013;54:585–591.
70. Duncker T, Lee W, Tsang SH, et al. Distinct characteristics of inferonasal fundus autofluorescence patterns in stargardt disease and retinitis pigmentosa. *Invest Ophthalmol Vis Sci*. 2013;54:6820–6826.
71. Pilotto E, Guidolin F, Convento E, et al. Fundus autofluorescence and microperimetry in progressing geographic atrophy secondary to age-related macular degeneration. *Br J Ophthalmol*. 2013;97:622–626.
72. Yoshitake S, Murakami T, Horii T, et al. Qualitative and quantitative characteristics of near-infrared autofluorescence in diabetic macular edema. *Ophthalmology*. 2014;121:1036–1044.
73. Curcio CA, Sloan KR, Kalina RE, Hendrickson AE. Human photoreceptor topography. *J Comp Neurol*. 1990;292:497–523.
74. Chen C, Tsina E, Cornwall MC, Crouch RK, Vijayaraghavan S, Koutalos Y. Reduction of all-trans retinal to all-trans retinol in the outer segments of frog and mouse rod photoreceptors. *Biophys J*. 2005;88:2278–2287.
75. Han M, Giese G, Schmitz-Valckenberg S, et al. Age-related structural abnormalities in the human retina-choroid complex revealed by two-photon excited autofluorescence imaging. *J Biomed Opt*. 2007;12:024012.
76. Fishman GA, Farber MD, Derlacki DJ. X-linked retinitis pigmentosa. Profile of clinical findings. *Arch Ophthalmol*. 1988;106:369–375.
77. Delori FC, Gragoudas ES, Francisco R, Pruett RC. Monochromatic ophthalmoscopy and fundus photography. The normal fundus. *Arch Ophthalmol*. 1977;95:861–868.
78. Delori FC, Pflibsen KP. Spectral reflectance of the human ocular fundus. *Appl Opt*. 1989;28:1061–1077.
79. Elsner AE, Burns SA, Weiter JJ, Delori FC. Infrared imaging of sub-retinal structures in the human ocular fundus. *Vision Res*. 1996;36:191–205.
80. van de Kraats J, Berendschot TT, van Norren D. The pathways of light measured in fundus reflectometry. *Vision Res*. 1996;36:2229–2247.
81. Jacobson SG, Cideciyan AV, Sumaroka A, et al. Remodeling of the human retina in choroideremia: rab escort protein 1 (REP-1) mutations. *Invest Ophthalmol Vis Sci*. 2006;47:4113–4120.
82. Lorenz B, Wabbels B, Wegscheider E, Hamel CP, Drexler W, Preising MN. Lack of fundus autofluorescence to 488 nanometers from childhood on in patients with early-onset severe retinal dystrophy associated with mutations in RPE65. *Ophthalmology*. 2004;111:1585–1594.
83. Katz ML, Redmond TM. Effect of Rpe65 knockout on accumulation of lipofuscin fluorophores in the retinal pigment epithelium. *Invest Ophthalmol Vis Sci*. 2001;42:3023–3030.
84. Tam BM, Moritz OL. Dark rearing rescues P23H rhodopsin-induced retinal degeneration in a transgenic Xenopus laevis model of retinitis pigmentosa: a chromophore-dependent mechanism characterized by production of N-terminally truncated mutant rhodopsin. *J Neurosci*. 2007;27:9043–9053.
85. Li ZY, Possin DE, Milam AH. Histopathology of bone spicule pigmentation in retinitis pigmentosa. *Ophthalmology*. 1995;102:805–816.
86. Jacobson SG, Cideciyan AV. Treatment possibilities for retinitis pigmentosa. *N Engl J Med*. 2010;363:1669–1671.
87. Jacobson SG, Roman AJ, Aleman TS, et al. Normal central retinal function and structure preserved in retinitis pigmentosa. *Invest Ophthalmol Vis Sci*. 2010;51:1079–1085.

Investigative Ophthalmology & Visual Science

88. Klein R, Klein BE, Franke T. The relationship of cardiovascular disease and its risk factors to age-related maculopathy. The Beaver Dam Eye Study. *Ophthalmology*. 1993;100:406–414.
89. Vingerling JR, Dielemans I, Hofman A, et al. The prevalence of age-related maculopathy in the Rotterdam Study. *Ophthalmology*. 1995;102:205–210.
90. von Rückmann A, Fitzke FW, Bird AC. Fundus autofluorescence in age-related macular disease imaged with a laser scanning ophthalmoscope. *Invest Ophthalmol Vis Sci*. 1997; 38:478–486.
91. Holz FG, Bellmann C, Margaritidis M, Schütt F, Otto TP, Völcker HE. Patterns of increased in vivo fundus autofluorescence in the junctional zone of geographic atrophy of the retinal pigment epithelium associated with age-related macular degeneration. *Graefes Arch Clin Exp Ophthalmol*. 1999;237:145–152.
92. Mauschitz MM, Fonseca S, Chang P, et al; for the GAP Study Group. Topography of geographic atrophy in age-related macular degeneration. *Invest Ophthalmol Vis Sci*. 2012;53: 4932–4939.
93. Bhisitkul RB, Mendes TS, Rofagha S, et al. Macular atrophy progression and 7-year vision outcomes in subjects from the ANCHOR, MARINA and HORIZON studies. (Study SEVEN-UP). *Am J Ophthalmol*. 2015;159:915–924, e2.
94. Boon CJ, Jeroen Klevering B, Keunen JE, Hoyng CB, Theelen T. Fundus autofluorescence imaging of retinal dystrophies. *Vision Res*. 2008;48:2569–2577.
95. Kaczurowski MI. The pigment epithelium of the human eye. *Am J Ophthalmol*. 1962;53:79–92.
96. Schmidt SY, Peisch RD. Melanin concentration in normal human retinal pigment epithelium. Regional variation and age-related reduction. *Invest Ophthalmol Vis Sci*. 1986;27: 1063–1067.
97. Hayasaka S. Aging changes in lipofuscin, lysosomes and melanin in the macular area of human retina and choroid. *Jpn J Ophthalmol*. 1989;33:36–42.
98. Gao H, Hollyfield JG. Aging of the human retina. Differential loss of neurons and retinal pigment epithelial cells. *Invest Ophthalmol Vis Sci*. 1992;33:1–17.
99. Hjelmeland LM, Fujikawa A, Oltjen SL, Smit-McBride Z, Braunschweig D. Quantification of retinal pigment epithelial phenotypic variation using laser scanning cytometry. *Mol Vis*. 2010;16:1108–1121.
100. Lois N, Halfyard AS, Bird AC, Fitzke FW. Quantitative evaluation of fundus autofluorescence imaged "in vivo" in eyes with retinal disease. *Br J Ophthalmol*. 2000;84:741–745.
101. Cideciyan AV, Swider M, Aleman TS, et al. ABCA4-associated retinal degenerations spare structure and function of the human parapapillary retina. *Invest Ophthalmol Vis Sci*. 2005; 46:4739–4746.
102. Delori F, Greenberg JP, Woods RL, et al. Quantitative measurements of autofluorescence with the scanning laser ophthalmoscope. *Invest Ophthalmol Vis Sci*. 2011;52:9379–9390.
103. Greenberg JP, Duncker T, Woods RL, Smith RT, Sparrow JR, Delori FC. Quantitative fundus autofluorescence in healthy eyes. *Invest Ophthalmol Vis Sci*. 2013;54:5684–5693.
104. Burke TR, Duncker T, Woods RL, et al. Quantitative fundus autofluorescence in recessive Stargardt disease. *Invest Ophthalmol Vis Sci*. 2014;55:2841–2852.
105. Norren DV, Vos JJ. Spectral transmission of the human ocular media. *Vision Res*. 1974;14:1237–1244.
106. Pokorny J, Smith VC, Lutze M. Aging of the human lens. *Appl Opt*. 1987;26:1437–1440.
107. Sample PA, Esterson FD, Weinreb RN, Boynton RM. The aging lens: in vivo assessment of light absorption in 84 human eyes. *Invest Ophthalmol Vis Sci*. 1988;29:1306–1311.
108. Van Best JA, Kuppens EV. Summary of studies on the blue-green autofluorescence and light transmission of the ocular lens. *J Biomed Opt*. 1996;1:243–250.
109. Owsley C, Jackson GR, Cideciyan AV, et al. Psychophysical evidence for rod vulnerability in age-related macular degeneration. *Invest Ophthalmol Vis Sci*. 2000;41:267–273.
110. Broendsted AE, Hansen MS, Lund-Andersen H, Sander B, Kessel L. Human lens transmission of blue light: a comparison of autofluorescence-based and direct spectral transmission determination. *Ophthalmic Res*. 2011;46:118–124.

Investigative Ophthalmology & Visual Science